Spectroscopic Examination, DFT Calculations, Electronic and Optical Properties of α-santonin

Palani Murugan, S. Jeyavijayan, K. Viswanathan

Abstract*: *In this work, the FTIR and FT-Raman spectra of α-santonin have been recorded and vibrational analysis of the compound were carried out from the observed data. The molecular parameters such as bond length, bond angle, frequencies and spectral intensities were estimated with the help of density functional theory (DFT/B3LYP) method. The calculated and experimental spectra were compared and the stability of the molecule has been studied by the natural bond orbital analysis. The electronic properties like HOMO-LUMO have also been analyzed. The nonlinear optical properties of the molecule have been analyzed by calculating the first hyperpolarisability and comparing with urea.

Keywords*:*FTIR; FT-Raman; DFT calculations; α-santonin.

I. INTRODUCTION

α-santonin consists of three isoprene units called sesquiterpene lactone and it is derived from the unexpanded flower-heads of Artemisia maritime, santonica. It exhibits several biological activities like anthelmintic, antipyretic, anti-inflammatory, and fungicidal. It has been chosen as the starting material for the synthesis of several biologically important molecules [1]. It has a highly functionalised ring with a cross conjugated dienone system and a lactone moiety. Recently, several santonin derivatives are known to exhibit significant anticancer activity [2]. Further, since α-santonin bears several reactive centres, it offers opportunity for further chemical modification of its scaffold to generate new secondary leads [3]. In solid-state organic chemistry, the secret behind the photoarrangement of α-santonin have been revealed by Natarajan et al. [4]. Literature survey reveals that no DFT frequency calculations for α-santonin have been reported so far. Because of these versatile importances of the α-santonin (ASN), the investigation of vibrational spectra, DFT calculations, electronic and optical properties of the title molecule has been undertaken in this study.

II. EXPERIMENTAL

The pure sample of ASN was used as such for recording the Fourier transform infrared spectrum in the region 4000-400 cm^{-1}, using Perkin Elmer FTIR spectrometer. The FT-Raman spectrum of ASN is recorded on BRUKER RFS 66V model interferometer equipped with FRA-106 FT-Raman accessories in the Stokes region 3500-50 cm^{-1} using Nd: YAG laser operating at 200 mW power continuously with 1064 nm excitation. The structural characteristics and the normal vibrational modes of ASN have been carried out using the DFT-B3LYP correlation functional using the GAUSSIAN 09W software package [5]. Initially, the Becke 3LYP keyword, which invokes Becke's three-parameter hybrid method [6] calculations, employing the correlation function of Lee et al. [7], adopting the lower basis set 6-31+G(d,p) are carried out and then the DFT/B3LYP implemented with higher basis set 6-311++G(d,p) have been carried out. According to SQM procedure [8], the scaling of the force constants were performed. The calculation of the total energy distribution (TED) are done on a PC with the MOLVIB program (version V7.0-G77) written by Sundius [9]. By the use of GAUSSVIEW molecular visualization program [10] along with available related molecules, the vibrational frequency assignments were made by their TED with a high degree of confidence.

III. RESULT AND DISCUSSION

The optimized molecular structure of ASN is shown in Fig. 1. The optimization geometrical parameters of ASN obtained by the DFT/B3LYP method with 6-31+G(d,p) and 6-311++G(d,p) basis sets in comparison with the experimental data [11] are presented in the Table I. The rings of ASN appears little distorted and angles slightly out of perfect hexagonal structure. It is due to the substitutions of the methyl groups and carbonyl groups in the place of H atoms. The rings with C12–C13, C9–C11, C6–C13 and C1–C2 bond lengths exactly at the substitution place are 1.492, 1.343, 1.362 and 1.533Å (cal. by B3LYP/6-31+G(d,p)), respectively differ from the remaining bonds (~1.5 cal.) in the ring. The C=O bond length indicates a considerable increase when substituted in place of C–H and are in good agreement with experimental results. According to the DFT calculations, the bond angle C2–C1–O28, C11–C12–C13, C8–C7–C9, C6–C13–C12 and C1–C2–C3 are found to be 110.01, 118.93, 107.10, 119.54 and 101.54 (cal. by B3LYP/6-31+G(d,p)), respectively, and are deviated from 1200, where the substitutions of the methyl groups and carbonyl groups in the place of hydrogen. From the structural point of view, the molecule is assumed to have C1 point group symmetry, consists of 36 atoms and expected to have 102 normal modes of vibrations.

The detailed vibrational assignments of fundamental modes of ASN along with the TED % are given in Table II. The observed and calculated FTIR and FT-Raman spectra of ASN are shown in Figs. 2 and 3, respectively. The main focus of the present investigation is the proper assignment of the experimental frequencies to the various vibrational

Revised Manuscript Received on December 20, 2019.
***** Correspondence Author
Palani Murugan, Department of Physics, Dr. B.R. Ambedkar Institute of Technology, Port Blair-744103, Andaman & Nicobar Islands, India Email : palanimuruganviji@gmail.com
S. Jeyavijayan*, Department of Physics , Kalasalingam Academy of Research and Education, Krishnankoil-626 126, Tamil Nadu, India Email : sjeyavijayan@gmail.com
K. Viswanathan, Department of Physics, Kalasalingam Academy of Research and Education, Krishnankoil-626 126, Tamil Nadu, India Email : kvnooty@gmail.com

modes of ASN in collaboration with the calculated harmonic vibrational frequencies at B3LYP level using the standard 6-31+G(d,p) and 6-311++G(d,p) basis sets. The results indicate that the B3LYP/6-311++G(d,p) calculations approximate the observed fundamental frequencies much better than the B3LYP/6-31+G(d,p) results. The vibrational analysis obtained for ASN with the unscaled B3LYP force field is generally somewhat greater than the experimental values. Therefore, the calculated frequencies were scaled by using scaling factor of 0.9613 for B3LYP method [12]. The resultant scaled frequencies are also listed in Table II.

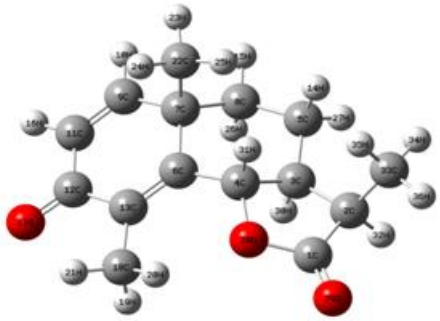

Figure 1. Molecular structure of α-santonin

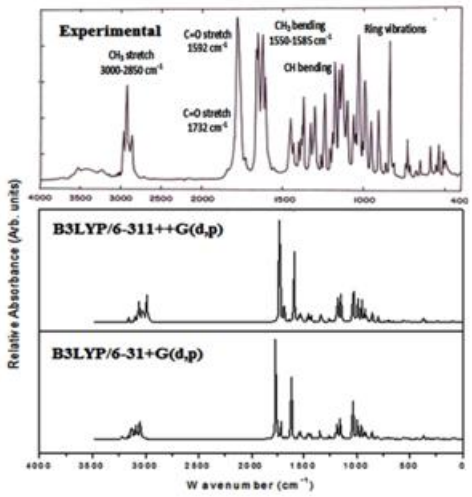

Figure 2.IR spectra of α-santonin

C-H Vibrations

Aromatic compounds commonly exhibit multiple weak bands in the region 3100-3000 cm^{-1} due to aromatic C-H stretching vibrations [13]. Hence, the Raman bands appeared at 3250, 3150, 3104 and 3042 cm^{-1} and the IR band found at 3078 cm^{-1} in ASN have been assigned to C-H stretching vibrations and these modes are confirmed by their TED values. The bands due to C-H in-plane ring bending vibrations, interact somewhat with C-C stretching vibrations, are observed as a number of sharp bands in the region 1300-1000 cm^{-1}. The C-H out-of-plane bending vibrations are strongly coupled vibrations and occur in the region 900-667 cm-1. The FT-Raman bands at 942, 928, 870 cm^{-1} and infrared bands at 905, 862 cm^{-1} are assigned to C–H in-plane bending vibrations of ASN. The out-of-plane bending vibrations of C-H group have also been identified for ASN and they are presented in Table II.

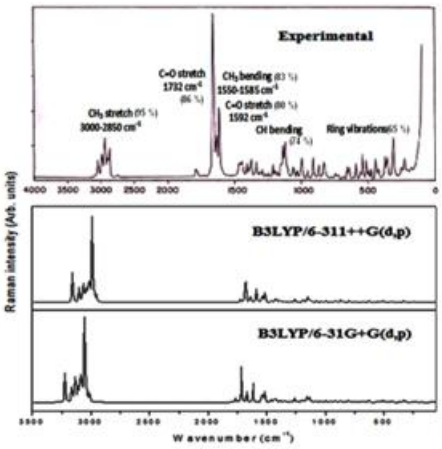

Figure 3.Raman spectra of α-santonin

C=O Vibrations

The carbonyl group vibrational frequencies are the significant characteristic bands in the vibrational spectra of ketones, and for this reason, such bands have been the subject of extensive studies [14]. The carbonyl stretching vibrations in ketones are expected in the region 1680–1715 cm^{-1}. In this case, the band observed at 1785, 1738 cm^{-1} in FT-Raman spectrum is assigned as C=O stretching vibration. The vibrational bands at 834, 820 cm^{-1} and 320, 250 cm^{-1} are assigned to C=O in-plane and out-of-plane bending vibrations for ASN, respectively. These vibrational assignments are in line with the literature [14].

C–C Vibrations

The C-C aromatic stretching vibrations gives rise to characteristic bands in both the observed IR and Raman spectra [15], covering the spectral range from 1600 to 1400 cm^{-1}. Therefore, the C-C stretching vibrations of ASN are found at 1700, 1640, 1610, 1475, 1450, 1160, 1145, 1125, 1068 cm^{-1} in FTIR and 1665, 1652, 1625, 1618, 1575, 1168, 1138, 1095, 1062 cm^{-1} in the FT-Raman spectrum and these modes are confirmed by their TED values. Most of the ring vibrational modes are affected by the substitutions in the aromatic ring of ASN. In the present study, the bands observed at 720, 690, 660, 640, 605 cm^{-1} and 695, 652, 590 cm^{-1} in the FTIR and Raman spectrum, respectively, have been designated to ring in-plane bending modes by careful consideration of their quantitative descriptions. The ring out-of-plane bending modes of ASN are also listed in the Table II.

CH_3 Vibrations

For the assignments of CH_3 group frequencies, nine fundamental vibrations can be associated to each CH_3 group. Three stretching, three bending, two rocking modes and single torsional mode describe the motion of the methyl group. In this study, the CH_3 symmetric stretch frequencies are established at 2890, 2852 cm^{-1} in IR and 2898 cm^{-1} in Raman spectra. The CH_3 in-plane stretch frequencies are assigned at 3015, 3010, 3000 cm^{-1} in Raman spectra for the title compound.

These assignments are also supported by the literature [16] in addition to TED output. We have observed the symmetrical methyl deformation mode at 1355, 1318, 1310 cm^{-1} in the IR and Raman spectrum. The band at 2996, 2974, 2960 cm^{-1} and 1400, 1396, 1388 cm^{-1} in the experimental spectra are attributed to CH_3 out-of-plane stretching and out-of-plane bending modes, respectively. The methyl deformation modes mainly coupled with in-plane bending vibrations. The bands obtained at 1026, 1020, 1000 and 1278, 1272, 1250 cm^{-1} are assigned to CH_3 in-plane and out-of-plane rocking modes, respectively. The assignment of the band at 235, 210, 135 cm^{-1} in IR is attributed to methyl twisting mode.

CH_2 Vibrations

For the assignment of CH_2 group frequencies basically six fundamental can be associated to each CH_2 group. The asymmetric CH_2 stretching vibrations [17] are generally observed below 3000 cm^{-1}, and the symmetric stretch will appear between 3000 and 2700 cm^{-1}. In this study, the asymmetric and symmetric stretching vibrations are observed at 2920, 2902 cm^{-1} and 2780, 2752 cm^{-1} in the experimental IR and Raman spectra. They are very pure modes since their TED contributions are above 90%. The CH_2 in-plane and out-of-plane bending modes are assigned at 1382, 1363 and 1240, 1195 cm^{-1}, respectively. The CH_2 in-plane and out-of-plane rocking modes are observed at 992, 950 and 1180, 1175 cm^{-1}, respectively. These modes are in good agreement with the calculated results.

Table I.Optimized geometrical parameters of α-santonin obtained by DFT-B3LYP method

Bond length	Value (Å)		[a]Expt	Bond angle	Value (°)		Expt[11]
	B3LYP/ 6-31+G(d,p)	B3LYP/ 6-311++G(d,p)			B3LYP/ 6-31+G(d,p)	B3LYP/ 6-311++G(d,p)	
C1-C2	1.533	1.530	1.524	C2-C1-O28	110.01	109.94	-
C1-O28	1.402	1.401	1.357	C2-C1-O29	128.52	128.58	-
C1-O29	1.224	1.221	1.198	O28-C1-O29	121.46	121.48	-
C2-C3	1.545	1.543	1.535	C1-C2-C3	101.54	101.58	100.7
C2-H32	1.095	1.091	-	C1-C2-H32	107.89	107.80	-
C2-C33	1.545	1.543	1.514	C1-C2-H33	110.70	110.70	-
C3-C4	1.549	1.546	1.531	C3-C2-H32	111.51	111.39	-
C3-C5	1.528	1.526	1.514	C3-C2-C33	116.11	116.16	
C3-H30	1.101	1.097	-	H32-C2-C33	108.68	108.77	-
C4-C6	1.510	1.509	1.516	C2-C3-C4	102.68	102.68	101.1
C4-O28	1.483	1.481	1.440	C2-C3-C5	121.62	121.79	
C4-H31	1.098	1.093	-	C2-C3-H30	107.23	107.00	-
C5-C8	1.545	1.543	1.528	C4-C3-C5	109.98	110.11	109.4
C5-H14	1.098	1.093	-	C4-C3-H30	106.39	106.22	-
C5-H27	1.098	1.093	-	C5-C3-H30	107.97	108.03	-
C6-C7	1.548	1.547	1.527	C3-C4-C6	111.18	111.17	110.4
C6-C13	1.362	1.357	1.336	C3-C4-O28	102.85	102.84	104.2
C7-C8	1.578	1.576	1.556	C3-C4-H31	109.74	109.65	-
C7-C9	1.507	1.506	1.496	C6-C4-O28	118.53	118.42	
C7-C22	1.569	1.566	1.564	C6-C4-H31	109.14	109.20	-
C8-H15	1.098	1.093	-	C3-C5-H14	104.96	105.12	-
C8-H26	1.098	1.094	-	C3-C5-C8	108.43	108.48	107.1
C9-H10	1.089	1.086	-	C8-C5-H14	110.76	110.76	-
C9-C11	1.343	1.338	1.320	C3-C5-H27	110.86	110.89	-
C11-C12	1.466	1.465	1.460	C8-C5-H14	110.80	110.82	-
C11-H16	1.085	1.082	-	C8-C5-H27	109.20	109.16	-
C12-C13	1.492	1.491	1.487	H14-C5-H27	106.78	106.72	-
C12-O17	1.258	1.256	1.223	C4-C6-C7	109.21	109.32	109.7
C13-C18	1.511	1.510	1.507	C4-C6-C13	127.55	127.38	
C18-H19	1.098	1.094	-	C7-C6-C13	123.23	123.29	123.9
C18-H20	1.086	1.082	-	C6-C7-C8	110.77	110.79	112.2
C18-H21	1.095	1.090	-	C6-C7-C9	112.76	112.71	112.0
C22-H23	1.096	1.092	-	C6-C7-C22	110.22	110.08	
C22-H24	1.095	1.090	-	C8-C7-C9	107.10	107.10	
C22-H25	1.094	1.090	-	C8-C7-C22	109.63	109.70	
C33-H34	1.095	1.091	-	C9-C7-C22	106.19	106.31	
C33-H35	1.096	1.092	-	C5-C8-C7	114.60	114.69	114.3
C33-H36	1.095	1.090	-	C5-C8-H15	110.28	110.29	-
				C5-C8-H26	108.80	108.83	-
				C7-C8-H15	108.11	108.11	-
				C7-C8-H26	107.81	107.75	-
				H15-C8-H26	106.95	106.86	-
				C7-C9-H10	115.49	115.54	-
				C7-C9-C11	123.95	123.92	124.6
				H10-C9-C11	120.55	120.54	-
				C9-C11-C12	121.32	121.41	121.2
				C9-C11-H16	122.44	122.44	-
				C12-C11-H16	116.24	116.14	-
				C11-C12-C13	118.93	118.89	118.1
				C11-C12-O17	120.24	120.22	
				C13-C12-O17	120.82	120.89	
				C6-C13-C12	119.54	119.48	119.6

C6-C13-C18	126.81	126.70	
C12-C13-C18	113.65	113.82	
C1-O28-C4	109.12	109.13	109.5
C2-C33-H34	110.33	110.41	-
C2-C33-H35	112.11	112.17	-
C2-C33-H36	109.91	109.97	-
H34-C33-H35	108.21	108.16	-
H34-C33-H36	108.29	108.24	-
H35-C33-H36	107.87	107.76	-

Table II. The observed FTIR, FT Raman and calculated (unscaled and scaled) frequencies (cm^{-1}), IR intensity (km mol^{-1}), Raman activity ($Å^4amu^{-1}$) and probable assignments (Characterized by TED) for α-santonin using B3LYP method

Observed fundamentals (cm^{-1})		Calculated frequencies ν_i (cm^{-1})								TED(%) among types of internal coordinates
		B3LYP/6-31+G(d,p)				B3LYP/6-311++G(d,p)				
FTIR	Raman	Unscaled ν_i	Scaled	IR intensity	Raman activity	Unscaled ν_i	Scaled	IR Intensity	Raman activity	
-	3250(w)	3226	3097	2.70	29.07	3156	3030	12.33	145.13	CH stretching (99)
-	3150(w)	3218	3089	11.33	192.00	3155	3029	2.57	70.47	CH stretching (98)
-	3104(w)	3161	3035	18.35	111.31	3099	2975	18.94	105.50	CH stretching (97)
3078 (s)	-	3139	3013	22.07	53.78	3071	2948	22.76	51.42	CH stretching (99)
-	3042(w)	3136	3011	16.51	91.59	3067	2944	18.61	84.69	CH stretching (98)
-	3015(w)	3127	3002	32.37	45.27	3059	2937	34.55	43.45	CH_3 in-plane stretching (97)
-	3010(w)	3124	2999	24.71	68.96	3057	2935	25.87	64.67	CH_3 in-plane stretching (96)
-	3000(w)	3106	2982	11.99	90.49	3040	2918	14.02	89.28	CH_3 in-plane stretching (94)
2996(w)	-	3093	2969	50.72	61.71	3028	2907	50.94	56.42	CH_3 out-of-plane stretching (92)
-	2974(w)	3087	2964	1.84	104.43	3020	2899	2.02	109.96	CH_3 out-of-plane stretching (93)
2960(w)	-	3078	2955	24.01	103.73	3012	2892	25.57	100.67	CH_3 out-of-plane stretching (94)
2920(w)	-	3055	2933	71.01	397.08	2991	2871	58.06	498.86	CH_2 asymmetric stretching (95)
-	2902(w)	3053	2931	17.80	172.16	2990	2870	28.96	105.58	CH_2 asymmetric stretching (94)
-	2898(w)	3051	2929	4.20	44.50	2987	2868	2.54	30.19	CH_3 symmetric stretching (92)
2890(w)	-	3047	2925	1.52	46.56	2982	2863	1.94	50.72	CH_3 symmetric stretching (91)
2852(w)	-	3045	2923	18.09	45.90	2981	2862	14.78	30.01	CH_3 symmetric stretching (92)
2780(vw)	-	3037	2916	22.71	52.44	2972	2853	21.50	46.29	CH_2 symmetric stretching (90)
-	2752(w)	3015	2894	4.69	60.23	2951	2833	4.64	55.31	CH_2 symmetric stretching (90)
-	1785(ms)	1763	1692	413.89	17.77	1727	1658	408.10	16.90	C=O stretching (89)
-	1738(vs)	1716	1647	70.54	149.49	1683	1616	72.86	155.43	C=O stretching (90)
1700(s)	-	1672	1605	8.09	42.99	1641	1575	7.60	35.08	C-C stretching (88)
-	1665(vs)	1617	1552	248.77	75.30	1588	1524	232.26	66.76	C-C stretching (85)
-	1652(vs)	1546	1484	8.28	4.74	1544	1482	7.86	4.75	C-C stretching (87)
1640(s)	-	1541	1479	5.88	4.38	1540	1478	4.12	2.90	C-C stretching (86)
-	1625(vs)	1538	1476	11.80	17.62	1538	1476	8.16	7.36	C-C stretching (85)
-	1618(vs)	1537	1476	11.29	7.77	1536	1475	11.64	14.09	C-C stretching (84)
1610(s)	-	1532	1471	4.11	7.58	1531	1470	6.32	10.21	C-C stretching (84)
-	1575(s)	1532	1471	12.43	4.53	1530	1469	8.83	2.51	C-C stretching (83)
1475(w)	-	1521	1460	4.38	9.61	1518	1457	6.13	6.86	C-C stretching (82)
1450(w)	-	1517	1456	7.96	37.45	1516	1455	10.11	46.86	C-C stretching (80)
-	1430(s)	1463	1404	15.91	9.77	1465	1406	17.53	8.93	CH_3 in-plane bending (78)
1424(w)	-	1453	1395	4.91	3.84	1450	1392	12.50	0.44	CH_3 in-plane bending (79)
-	1415(s)	1452	1394	19.90	1.68	1448	1390	10.88	3.48	CH_3 in-plane bending (76)
1400(w)	-	1434	1377	21.02	7.46	1429	1372	21.75	7.78	CH_3 out-of-plane bending (75)
-	1396(s)	1427	1370	1.77	8.22	1424	1367	1.76	10.00	CH_3 out-of-plane bending (76)
1388(vw)	-	1417	1360	0.89	15.16	1413	1356	0.98	13.25	CH_3 out-of-plane bending (74)
-	1382(s)	1393	1337	2.19	1.35	1392	1336	1.10	1.76	CH_2 in-plane bending (75)
-	1363(s)	1387	1332	3.76	6.63	1388	1332	4.73	6.72	CH_2 in-plane bending (74)
1355(vw)	-	1379	1324	0.47	6.44	1377	1322	0.43	7.91	CH_3 symmetric bending (75)
-	1318(ms)	1355	1301	1.94	4.52	1354	1300	1.46	4.18	CH_3 symmetric bending (72)
1310(w)	-	1344	1290	33.31	4.66	1334	1281	32.45	5.20	CH_3 symmetric bending (73)
-	1278(vs)	1330	1277	3.60	1.77	1326	1273	4.20	1.62	CH_3 out-of-plane rocking (74)
1272(s)	-	1314	1261	1.95	3.17	1314	1261	0.98	3.58	CH_3 out-of-plane rocking (74)
1250(s)	-	1289	1237	1.78	5.69	1293	1241	1.17	5.73	CH_3 out-of-plane rocking (72)
-	1240(ms)	1259	1209	12.74	15.04	1258	1208	11.94	14.33	CH_2 out-of-plane bending (71)
-	1195(s)	1237	1188	8.49	4.18	1237	1188	6.96	3.51	CH_2 out-of-plane bending (72)
-	1180(s)	1201	1153	26.95	9.10	1193	1145	24.20	9.39	CH_2 out-of-plane rocking (72)
-	1175(s)	1192	1144	8.49	2.53	1188	1140	4.74	2.65	CH_2 out-of-plane rocking (70)
-	1168(s)	1181	1134	67.38	6.94	1177	1130	71.11	5.84	C-C stretching (75)
1160(w)	-	1156	1110	7.98	13.97	1153	1107	12.56	10.10	C-C stretching (71)
1145(w)	-	1155	1109	64.70	2.67	1149	1103	8.43	13.46	C-C stretching (72)
-	1138(s)	1150	1104	15.18	12.63	1145	1099	1.69	6.56	C-C stretching (72)
1125(w)	-	1135	1090	5.28	16.50	1131	1086	2.60	14.08	C-C stretching (71)
-	1095(w)	1116	1071	4.32	4.58	1111	1067	2.96	4.49	C-C stretching (74)
1068(s)	-	1093	1049	0.26	1.10	1095	1051	0.20	1.56	C-C stretching (75)
-	1062(ms)	1081	1038	3.82	6.88	1077	1034	2.36	7.73	C-C stretching (72)
-	1052(ms)	1050	1008	3.43	3.22	1050	1008	4.14	3.22	C-O stretching (70)
-	1036(ms)	1045	1003	0.97	0.90	1047	1005	1.06	0.78	C-O stretching (71)

1026(s)	-	1036	995	149.56	4.01	1032	991	155.51	4.47	CH_3 in-plane rocking (74)
-	1020(ms)	1018	977	5.18	3.04	1010	970	4.64	2.80	CH_3 in-plane rocking (72)
1000(ms)	-	1003	963	6.05	2.03	1002	962	6.70	1.70	CH_3 in-plane rocking (70)
-	992(w)	993	953	82.35	6.64	989	949	83.64	7.27	CH_2 in-plane rocking (69)
950(ms)	-	956	918	77.80	5.32	950	912	77.15	5.13	CH_2 in-plane rocking (70)
-	942(vs)	927	890	35.12	3.03	925	888	37.93	2.51	C-H in-plane bending (71)
-	928(ms)	917	880	0.49	3.08	915	878	1.01	3.71	C-H in-plane bending (70)
905(ms)	-	912	876	21.39	5.20	908	872	21.57	4.52	C-H in-plane bending (71)
-	870(s)	871	836	10.79	7.84	869	834	10.04	8.51	C-H in-plane bending (72)
862(ms)	-	856	822	32.95	1.43	852	818	34.80	1.82	C-H in-plane bending (70)
-	834(ms)	844	810	1.27	3.12	843	809	1.27	3.00	C=O in-plane bending (72)
-	820(ms)	802	770	14.83	8.26	791	759	16.93	7.97	C=O in-plane bending (69)
810(ms)	-	754	724	0.10	2.58	751	721	0.25	2.54	C-H out-of-plane bending (69)
-	760(s)	739	709	5.39	0.60	736	707	3.74	0.64	C-H out-of-plane bending (68)
-	750(s)	722	693	3.96	1.51	720	691	2.85	1.79	C-H out-of-plane bending (65)
-	745(s)	700	672	5.78	2.12	697	669	7.85	2.55	C-H out-of-plane bending (64)
738(vs)	-	680	653	3.38	4.43	676	649	2.79	3.78	C-H out-of-plane bending (66)
720(vw)	-	658	632	2.78	0.55	656	630	3.08	0.59	Ring in-plane bending (69)
-	695(w)	628	603	1.73	7.54	628	603	1.63	6.99	Ring in-plane bending (70)
690(w)	-	559	537	5.81	2.05	559	537	6.50	1.73	Ring in-plane bending (71)
660(w)	-	547	525	3.01	4.83	548	526	2.84	4.64	Ring in-plane bending (69)
-	652(ms)	523	502	4.64	2.89	524	503	4.59	3.64	Ring in-plane bending (68)
640(w)	-	510	490	3.91	6.35	511	491	3.73	5.86	Ring in-plane bending (70)
605(w)	-	488	468	0.33	3.14	491	471	0.35	3.53	Ring in-plane bending (71)
-	590 (ms)	438	420	2.10	3.04	439	421	2.00	3.24	Ring in-plane bending (71)
560(w)	-	430	413	0.83	4.96	429	412	0.85	4.98	C-C in-plane bending (68)
552(w)	-	372	357	12.08	0.62	373	358	12.13	0.62	C-C in-plane bending (69)
-	545(s)	364	349	2.45	1.04	368	353	`1.81	0.97	C-C in-plane bending (66)
532(ms)	-	331	318	1.60	5.63	337	324	0.87	0.97	Ring out-of-plane bending (65)
-	526(s)	326	313	0.34	2.96	333	320	1.23	8.02	Ring out-of-plane bending (62)
515(ms)	-	321	308	1.83	4.19	324	311	1.63	3.54	Ring out-of-plane bending (64)
490(w)	-	275	264	1.76	0.53	324	311	0.25	0.23	Ring out-of-plane bending (65)
-	482(ms)	254	244	1.28	0.13	295	283	0.48	0.44	Ring out-of-plane bending (66)
-	476(vw)	248	238	0.86	0.88	272	261	1.30	0.52	Ring out-of-plane bending (62)
445(w)	-	235	226	1.95	1.42	246	236	2.45	1.60	Ring out-of-plane bending (63)
-	436(w)	227	218	1.33	1.26	240	230	1.85	1.34	Ring out-of-plane bending (64)
410(w)	412(w)	216	207	0.42	0.78	232	223	0.84	1.03	C-C out-of-plane bending (62)
372(w)	375(w)	183	176	0.53	0.83	205	197	0.37	1.22	C-C out-of-plane bending (61)
360(w)	358(w)	179	172	0.59	0.53	192	184	0.78	1.09	C-C out-of-plane bending (64)
320(w)	-	109	105	0.53	0.87	180	173	0.27	0.42	C=O out-of-plane bending (62)
250(w)	-	97	93	3.38	0.99	189	181	1.68	1.58	C=O out-of -plane bending (61)
235(w)	-	84	81	3.38	0.76	95	91	3.94	0.49	CH_3 twisting (59)
210(w)	-	65	62	1.65	1.37	75	72	2.01	1.30	CH_3 twisting (57)
135(w)	-	51	49	0.45	1.13	65	62	0.72	0.87	CH_3 twisting (56)

The quantum chemistry based on the prediction of non-linear optical (NLO) properties of a molecule has an important role for the design of materials in modern communication technology, signal processing and optical interconnections [18]. Especially organic molecules are studied because of their larger NLO susceptibilities arising π-electron cloud movement from donor to acceptor, fast NLO response times, high laser damage thresholds and low dielectric constants. The calculated values of total static dipole moment μ, the average linear polarizability, the anisotropy of the polarizability Δα, and the first hyperpolarizability β using the DFT method are 8.5071 Debye, 26.446 Å3, 56.5463 Å3 and 4.237×10-30 cm^5 $e.s.u.^{-1}$, respectively. The values of μ and β obtained by Sun et al. [19] with the B3LYP/6-311++G(d,p) method for urea are 1.373 Debye and 3.729×10-31 cm^5 $e.s.u.^{-1}$, respectively. The first hyperpolarizability of ASN is greater than 11 times that of urea. According to the magnitude of the first hyperpolarizability, the title compound may be a potential applicant in the development of NLO materials.

The highest occupied molecular orbitals (HOMOs) and the lowest-lying unoccupied molecular orbitals (LUMOs) play an important role in the electric and optical properties, as well as in UV–vis spectra and chemical reactions [20]. The atomic orbital HOMO and LUMO compositions of the frontier molecular orbital for ASN computed at the B3LYP/6-311++G(d,p) are shown in Fig. 4. The LUMO: of π nature, (i.e. benzene ring) is delocalized over the whole C-C bond of the dienone system. By contrast, the HOMO is located over the lactone group; consequently the HOMO → LUMO transition implies an electron density transfer from lactone group to dienone system. The HOMO–LUMO energy gap of ASN at B3LYP method using 6-311++G(d,p) basis set is calculated as 4.763 eV, which reveals that the energy gap reflects the chemical activity of the molecule.The interpretation of quantum chemical results, in terms of chemically significant terms, can be done using Natural Bond Orbital (NBO) analysis. In the present study, the NBO calculations were performed on ASN using NBO 3.1 program as implemented in the Gaussian 09 package at the DFT/B3LYP.

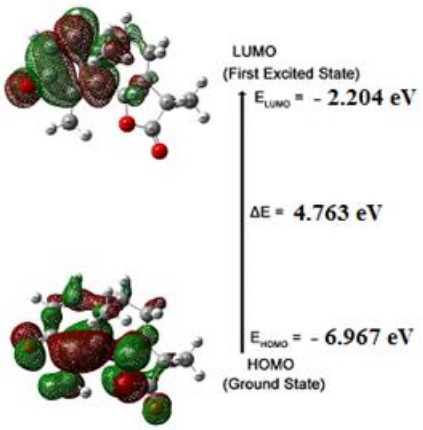

Figure 4. The atomic orbital HOMO and LUMO compositions for α-santonin

This helps to know the different molecular interactions between the filled and vacant orbitals, which is the measure of the delocalization. In this study, the hyperconjugative interaction energy was deduced from the second-order perturbation approach [21]. The intramolecular charge transfer is one of the strongest causes for NLO activity. The second order perturbation theory analysis of Fock matrix in NBO basis of ASN indicates the intramolecular interactions due to the orbital overlap of σ (C3-H30) with σ*(C9-C11), causing stabilization of 1455.58 kcal/mol and overlap of σ(C7-C8) with σ*(C9-C11), leading stabilization of 1579.14 kcal/mol to the system. Similarly, the charge transfer from σ(C12-C13) to (σ*C9-C11) amounts to the stabilization of 6539.64 kcal/mol and the charge transfer from σ(C33-H36) to σ*(C13-C18) amounts to the stabilization of 4158.41 kcal/mol. These interactions are responsible for a pronounced decrease of the lone pair orbital occupancy than the other occupancy, and there is a possibility for hyper conjugation between carbon, oxygen atoms and the aromatic ring.

IV. CONCLUSION

The optimized geometries, harmonic vibrational wavenumbers and intensities of vibrational bands of α-santonin have been carried out. The theoretical results are compared with the experimental vibrations. The TED calculation regarding the normal modes of vibration provides a strong support for the frequency assignment. The calculated HOMO and LUMO energies shows that charge transfer occur within the molecule. The charge transfer, mainly due to the interaction from σ(C12-C13) → (σ*C9-C11) and n2(O17) → σ*(C11-H16), is reflected in the NBO results. Furthermore, the first hyperpolarizability of ASN has been calculated and the results are discussed. These results indicate that the α-santonin compound is a good candidate of nonlinear optical materials.

REFERENCES

1. B. Singh, J.S. Srivastava, R.L. Khosa and U.P. Singh, "Individual and combined effects of berberine and santonin on spore germination of some fungi," Folia Microbiol., vol. 46, pp. 137-142, 2001.
2. J. Khazir, P.P. Singh, D.M. Reddy, I. Hyder, S. Shafi, S.D. Sawant, G. Chashoo, A. Mahajan, M.S. Alam, A.K. Saxena, S. Arvinda, B.D. Gupta and H.M.S. Kumar, "Synthesis and anticancer activity of novel spiro-isoxazoline and spiro-isoxazolidine derivatives of α-santonin," Eur. J. Med. Chem., vol. 63, pp. 279-289, 2013.
3. F.F.P. Arantes, L.C.A. Barbosa, C.R.A. Maltha, A.J. Demuner, P.M. Costa, J.R.O. Ferreira, L.V. Costa-Lotufo, M.O. Moraes and C. Pessoa, "Synthesis of novel α-santonin derivatives as potential cytotoxic agents," Eur. J. Med. Chem., vol. 45, pp. 6045-6051, 2010.
4. A. Natarajan, C.K. Tsai, S.I. Khan, P. McCarren, K.N. Houk and M.A. Garcia-Garibay, "The Photoarrangement of α-Santonin is a Single-Crystal-to-Single-Crystal Reaction: A Long Kept Secret in Solid-State Organic Chemistry Revealed," J. Am. Chem. Soc., vol. 129, pp. 9846-9847, 2007.
5. H.J. Frisch, G.W. Trucks, H.B. Schlegel, G.E. Scuseria, M.A. Robb, J.R. Cheeseman, H.Nakatsuji, M. Caricato, X. Li, H.P. Hratchian, K. Toyota, R. Fukuda, J.Hasegawa, M. Ishida, R. Nakajima, Y. Honda, O. Kilao, H. Nakai, T. Verven, J. A. Montgomery Jr., J.E. Peralta, F. Ogliaro, M. Bearpark, J. J. Heyd, E. Brothers, K. N. Kudin, V.N. Staroverov, R. Kobayashi, J. Normand, K. Ragavachari, A. Rendell, J.C. Burant, S. J. Tomasi, M. Cossi, N. Rega, J. M. Millam, M. Klene, J. E. Knox, J. B. Cross, V. Bakken, C. Adamo, J. Jaramillo, R. Gomperts, R.E. Strattmann, O. Yazyev, A.J. Austin, R. Cammi, J.W. Ochetrski, R.L. Martin, K. Morokuma, V.G. Zakrazawski, G.A.Votn, P. Salvador, J.J. Dannenberg, S. Dapprich, A.D. Daniels, O. Farkas and J.B. Foresman, Gaussian O.G., Revision A.O2, Gaussian Inc., Wallingford, CT. 2009.
6. A.D. Becke, "Densityfunctional thermochemistry. III. The role of exact exchange," J. Chem. Phys., vol. 98, pp. 5648-5652, 1993.
7. C. Lee, W.Yang and R.G. Parr, "Development of the Colle-Salvetti correlation-energy formula into a functional of the electron density," Phys. Rev. B, vol. 37, pp. 785-789, 1988.
8. G. Rauhut and P. Pulay, "Transferable Scaling Factors for Density Functional Derived Vibrational Force Fields," J. Phys. Chem., vol. 99, pp. 3093-3100, 1995.
9. T. Sundius, Scaling of ab initio force fields by MOLVIB, Vib. Spectrosc., vol. 29, pp. 89-95, 2002.
10. A. Frisch, A.B. Nielson and A.J. Holder, Gaussview user manual, Gaussian Inc., Pittsburgh, PA, 2009.
11. C. Kitabayashi, Y. Matsuura, N. Tanaka, Y. Katsube and T. Matsuura, "Structure of α-santonin," Acta. Cryst., vol. C41, pp. 1779-1781, 1985.
12. D.C. Young, Computational Chemistry: A Practical Guide for Applying Techniques to Real World Problems (Electronic), John Wiley & Sons Ltd., New York, 2001.
13. S. George, Infrared and Raman characteristic group frequencies – Tables and Charts, Third ed., Wiley, Chichester, 2001.
14. B. Smith, Infrared Spectral Interpretation, A Systematic Approach, CRC Press, Washington, DC, 1999.
15. S. Ramalingam and S. Periandy, "Spectroscopic investigation, computed IR intensity, Raman activity and vibrational frequency analysis on 3-bromoanisole using HF and DFT (LSDA/MPW1PW91) calculations," Spectrochim. Acta A Mol. Biomol. Spectrosc., vol. 78, pp. 835-843, 2011.
16. N. Y. SugirthaSuni, L. GuruPrasad, and R. Ganapathi Raman Rajendran, "Vibrational Analysis and Non Linear Optical Activity of 3-fluoro-4-methylbenzonitrile," Orient. J. Chem., vol. 34(3), pp. 1638-1645, 2018.
17. P.P. Moorthi, S. Gunasekaran, S. Swaminathan, and G.R. Ramkumaar, "Quantum chemical density functional theory studies on the molecular structure and vibrational spectra of mannitol," Spectrochim. Acta A Mol. Biomol. Spectrosc., vol. 137, pp. 412-422, 2015.
18. D. Sajan, J. Hubert, V.S. Jayakumar and J. Zaleski, "Structural and electronic contributions to hyperpolarizability in methyl p-hydroxy benzoate," J. Mol. Struct., vol. 785, pp. 43-53, 2006.
19. Y.X. Sun, Q.L. Hao, W.X. Wei, Z.X. Yu, L.D. Lu, X. Wang and Y.S. Wang, Experimental and density functional studies on 4-(3,4-dihy droxybenzylideneamino)antipyrine, and 4-(2,3,4-trihydroxybenzylideneamino)antipyrine," J. Mol. Struct. (Theochem.), vol. 904, pp. 74-82, 2009.
20. I. Fleming, Frontier Orbitals and Organic Chemical Reactions, Wiley, London, 1976.
21. E.D. Glendening, J.K. Badenhoop, A.E. Reed, J.E. Carpenter, J.A.Bohmann, C.M. Morales and F.Weinhold, NBO 5.0, Theoretical Chemistry Institute, University of Wisconsin, Madison, 2001.

AUTHORS PROFILE

Palani Murugan has completed M.Sc from Bharathiar University, Coimbatore and M.Phil from Bharathidasan University, Tiruchirapalli. Presently working as Lecturer, Physics, in DR.B.R.Ambedkar Institute of Technology Port Blair since June 2012. Currently pursuing Ph.D from Kalasalingam Academy of Research and Education.

S. Jeyavijayan has completed M.Sc. and Ph.D. from Bharathidasan University, Trichirappalli in 2014. Currently working as Assistant Professor in Kalasalingam Academy of Research and Education from June 2015 onwards. Published more than 25 papers in National and International Journals. His fields of interest are Molecular Spectroscopy and Theoretical and Computational chemistry.

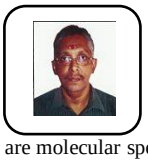

K. Viswanathan has completed M.Sc. and Ph.D. from University of Kerala Trivandrum in 1984 and worked in the High Energy Cosmic Ray group of TIFR for 22 years. Worked as Professor and HoD of Physics in Karpagam University for 10 years. Joined Kalasalingam University in August 2016 as Senior Professor. His fields of interest are molecular spectroscopy and Astroparticle physics at high energies.